

# TOF-SIMS imaging of adsorbed proteins on topographically complex surfaces with $\text{Bi}_3^+$ primary ions

B. J. Tyler<sup>a)</sup>

*Department of Chemical Engineering, University of the West Indies, Trinidad and Tobago*

C. Bruening

*Physikalisches Institut, University of Muenster, Germany*

S. Ranganarajan

*Department of Bioengineering, Duke University, Durham North Carolina*

H. F. Arlinghaus

*Physikalisches Institut, University of Muenster, Germany*

(Received 14 April 2011; accepted 30 June 2011; published 29 September 2011)

Although previous studies have demonstrated that TOF-SIMS is a powerful method for the characterization of adsorbed proteins due to its specificity and surface sensitivity, it was unclear from earlier work whether the differences between proteins observed on uniform flat surfaces were large enough to facilitate clear image contrast between similar proteins in small areas on topographically complex samples that are more typical of biological tissues. The goal of this study was to determine whether  $\text{Bi}_3^+$  could provide sufficiently high sensitivity to provide clear identification of the different proteins in an image. In this study, 10  $\mu\text{m}$  polystyrene microspheres were adsorbed with one of three different proteins, human serum albumin (HSA), bovine serum albumin (BSA), and hemoglobin. Spheres coated with HSA were then mixed with spheres coated with either BSA (a very similar protein) or hemoglobin (a dramatically different protein), and deposited on silicon substrates. Fluorescent labeling was used to verify the SIMS results. With maximum autocorrelation factors (MAF) processing, images showed clear contrast between both the very different proteins (HSA and hemoglobin) and the very similar proteins (HSA and BSA). Similar results were obtained with and without the fluorescent labels. MAF images were calculated using both the full spectrum and only characteristic amino acid fragments. Although better image contrast was obtained using the full spectrum, differences between the spheres were still evident when only the amino acid fragments were included in the analysis, suggesting that we are truly observing differences between the proteins themselves. These results demonstrate that TOF-SIMS, with a  $\text{Bi}_3^+$  primary ion, is a powerful technique for characterizing interfacial proteins not only on large uniform surfaces, but also with high spatial resolution on the topographically complex samples typical in biological analysis. © 2011 American Vacuum Society.

[DOI: 10.1116/1.3622347]

## I. INTRODUCTION

Interfacial proteins are of importance for a wide range of biological phenomena including cellular adhesion, cell signaling, and cell regulation. Research has found that adsorbed proteins play a key role in the performance of medical devices because they influence animal cell adhesion,<sup>1–3</sup> microbial infections,<sup>4–7</sup> calcification,<sup>8</sup> and tissue integration.<sup>9</sup> Additionally, the study of interfacial proteins is of growing importance in the areas of biosensors,<sup>10</sup> biofouling,<sup>11</sup> immunology,<sup>12</sup> and a host of biological processes.<sup>13–15</sup>

Interfacial proteins have been studied by a wide variety of techniques including antibody labeling,<sup>16</sup> ellipsometry,<sup>17</sup> x-ray photoelectron spectroscopy,<sup>18</sup> atomic force microscopy,<sup>19</sup> Fourier transform infrared spectroscopy,<sup>20</sup> near edge

x-ray adsorption fine structures, surface plasmon resonance, and time-of-flight secondary-ion mass spectroscopy.<sup>21</sup> In recent years, TOF-SIMS has become an increasingly important technique for the study of interfacial proteins because it has broader applicability and sensitivity than antibody binding based techniques and higher specificity and sensitivity than other spectroscopic techniques.<sup>18,21–27</sup>

Previous studies have demonstrated that TOF-SIMS is a powerful method for the characterization of adsorbed proteins due to its specificity and surface sensitivity. It has been demonstrated that TOF-SIMS can be used to identify pure proteins adsorbed to surfaces<sup>18,22,24</sup> to quantify the composition of mixed protein films<sup>25,27</sup> and to study the conformation of adsorbed proteins<sup>21,28,29</sup> and can provide relevant information in the study of synthetic biomaterials,<sup>30</sup> cells sheets,<sup>31</sup> and biosensors.<sup>10,32</sup> These earlier studies have, however, focused on large surface regions on which proteins are presumably uniformly adsorbed. From these studies, it is

<sup>a)</sup> Author to whom correspondence should be addressed; electronic mail: Prof.Bonnie@gmail.com

unclear whether the differences between proteins are large enough to facilitate clear image contrast between similar proteins in small areas. It is also unclear whether the differences will persist on topographically complex surfaces which are common in biological samples. Previously, we found that imaging of proteins adsorbed onto polystyrene microspheres with  $\text{Ga}^+$  primary ions failed to reveal distinct differences between proteins in the images because of the very low ionization probability for the amino acid specific fragments under  $\text{Ga}^+$  bombardment.<sup>33</sup>

In this study, we have used a  $\text{Bi}_3^+$  primary ion source to further this earlier attempt to image proteins adsorbed onto microspheres.<sup>33</sup> Numerous studies have shown that cluster ion sources including  $\text{Bi}_3^+$  can result in dramatic enhancements in both total ion yield and the yield of characteristic molecular ions<sup>34,35</sup> and suggest that this source will be more successful for imaging proteins than the older  $\text{Ga}^+$  primary ion sources.

## II. MATERIALS AND METHODS

### A. Sample preparation

Fluorescent microspheres, made of polystyrene and polystyrene divinylbenzene (red and green with 10  $\mu\text{m}$  mean diameter), were obtained from Duke Scientific Corporation, CA. Three different proteins: human serum albumin (HSA), bovine serum albumin (BSA), and bovine hemoglobin were obtained from Sigma–Aldrich, for adsorption onto the microspheres. The spheres were equilibrated in phosphate buffer (0.1 M) for 2 h before the adsorption. All the proteins were dissolved in phosphate buffer at 2000  $\mu\text{g}/\text{ml}$  and pipetted into the tubes containing the microspheres equilibrating in buffer to reach a protein concentration of 1000  $\mu\text{g}/\text{ml}$ . Protein adsorption was performed at 37 °C with this buffer for 4 h in an incubator-shaker to ensure uniform adsorption. After adsorption, the spheres were first washed in buffer to remove the loosely bound protein. They were then washed five times in deionized water to remove the buffer salts. For this study, BSA was adsorbed onto green microspheres and HSA and hemoglobin were adsorbed onto red microspheres.

Following adsorption and washing, green microspheres adsorbed with BSA were mixed with red microspheres which had been adsorbed with either HSA or hemoglobin, deposited on clean silicon wafers and air dried. Prior to TOF-SIMS analysis the samples were imaged in a fluorescent microscope. One additional study was performed where BSA, HSA, and hemoglobin were both adsorbed onto green microspheres.

### B. TOF-SIMS analysis

The samples were imaged using an Ion TOF IV spectrometer using a  $\text{Bi}_3^+$  primary ion beam with a 0.012 pA current and 100  $\mu\text{s}$  cycle time. The primary ion dose was limited to  $1 \times 10^{12}$  ions/ $\text{cm}^2$ . Images were collected in Ion TOF burst-alignment mode, in which the lens magnetization is set to zero to facilitate 300 nm spatial resolution. Samples were

TABLE I. Amino acid peaks.

Nominal mass	Fragment	Amino acid
30	$\text{CH}_4\text{N}^+$	glycine
43	$\text{CH}_3\text{N}_2^+$	arginine
44	$\text{C}_2\text{H}_6\text{N}^+$	alanine
60	$\text{C}_2\text{H}_6\text{NO}^+$	serine
61	$\text{C}_2\text{H}_5\text{S}^+$	methionine
68	$\text{C}_4\text{H}_6\text{N}^+$	proline
69	$\text{C}_4\text{H}_5\text{O}^+$	threonine
70	$\text{C}_3\text{H}_4\text{NO}^+, \text{C}_4\text{H}_8\text{N}^+$	asparagine, proline
71	$\text{C}_3\text{H}_3\text{O}_2^+$	serine
72	$\text{C}_4\text{H}_{10}\text{N}^+$	valine
73	$\text{C}_2\text{H}_7\text{N}_3^+$	arginine
74	$\text{C}_3\text{H}_8\text{NO}^+$	threonine
76	$\text{C}_2\text{H}_6\text{NS}^+$	cysteine
81	$\text{C}_4\text{H}_5\text{N}_2^+$	histidine
82	$\text{C}_4\text{H}_6\text{N}_2^+$	histidine
83	$\text{C}_5\text{H}_7\text{O}^+$	valine
84	$\text{C}_4\text{H}_6\text{NO}^+, \text{C}_5\text{H}_{10}\text{N}^+$	glutamine, glutamic acid, lysine
86	$\text{C}_5\text{H}_{12}\text{N}^+$	isoleucine, leucine
87	$\text{C}_3\text{H}_7\text{N}_2\text{O}^+$	asparagine
88	$\text{C}_3\text{H}_6\text{NO}_2^+$	aspartic acid, asparagine
98	$\text{C}_4\text{H}_4\text{NO}_2^+$	asparagine
100	$\text{C}_4\text{H}_{10}\text{N}_3^+$	arginine
101	$\text{C}_4\text{H}_{11}\text{N}_3^+$	arginine
102	$\text{C}_4\text{H}_8\text{NO}_2^+$	glutamic acid
107	$\text{C}_7\text{H}_7\text{O}^+$	tyrosine
110	$\text{C}_5\text{H}_8\text{N}_3^+$	histidine
112	$\text{C}_5\text{H}_8\text{N}_3^+$	arginine
120	$\text{C}_8\text{H}_{10}\text{N}^+$	phenylalanine
127	$\text{C}_5\text{H}_{11}\text{N}_4^+$	arginine
130	$\text{C}_9\text{H}_8\text{N}^+$	tryptophan
131	$\text{C}_9\text{H}_8\text{O}^+$	phenylalanine
136	$\text{C}_8\text{H}_{10}\text{NO}^+$	tyrosine
159	$\text{C}_{10}\text{H}_{11}\text{N}^+$	tryptophan
170	$\text{C}_{11}\text{H}_8\text{NO}^+$	tryptophan

analyzed using a 10 ns unbunched primary ion pulse to facilitate a mass resolution of approximately 1000 ( $\text{m}/\Delta\text{m}$ ).

### C. Multivariate image processing

Two data sets were extracted from each of the raw data image files using the IONTOF software package. The first stack of images was generated using a list of 321 peaks which included all peaks with greater than 50 counts in the total ion spectra except  $\text{Na}^+$ ,  $\text{K}^+$ , and  $\text{Ca}^+$ . These peaks were excluded to reduce variability arising from the buffer salts. The second stack of images was generated using a list of 34 peaks shown in Table I, which previous researchers have found are indicative of specific amino acids.<sup>24</sup>

Previous studies have found that multivariate statistical methods, such as principal components analysis (PCA) and linear discriminant analysis (LDA), are essential for extracting concise information from the complex TOF-SIMS spectra which arise from adsorbed protein films.<sup>22,24,36</sup> A related technique, maximum autocorrelation factors

(MAFs)<sup>37,38</sup> has proven to be valuable for processing images and has been applied in this work.

MAF is a variant of factor analysis that is closely related to the more widely used PCA. In PCA, the data matrix,  $X$ , is decomposed such that

$$S = XU^T, \quad (1)$$

where  $U$  is the loadings matrix and  $S$  is the scores matrix. The loadings matrix,  $U$ , can be obtained via an eigenvector rotation of the matrix  $X'X$ .<sup>12,13</sup> Unfortunately, PCA often yields less than satisfactory results when applied to low signal to noise ratio images so MAF has been used in this study. In MAF, the data matrix  $X$  is decomposed, as described in Eq. (2), however, the loadings matrix,  $U$ , is obtained by an eigenvector rotation of the matrix  $B$ .

$$B = A^{-1}X'X, \quad (2)$$

where  $A$  is the covariance matrix of the shift images. The shift images are obtained by subtracting the  $X$  matrix from a copy of itself that has been shifted by one pixel horizontally and/or one pixel vertically. The eigenvectors of matrix  $B$  which have the largest eigenvalues will identify linear combinations of ion peaks which maximize the variation across the entire image while minimizing the variation between neighboring pixels.<sup>37</sup> As with PCA, the scores can be displayed and interpreted as an image for an underlying component. The  $B$  matrix; however, is not symmetric so  $U$ , the loadings matrix, must be inverted to obtain the pseudospectra associated with the corresponding scores images.

Each of the image stacks assembled for this study, has been analyzed using MAF. The MAF images have been compared to fluorescence images to verify interpretation.

### III. RESULTS AND DISCUSSION

Figures 1 and 2 show images taken from two different samples of BSA and hemoglobin coated spheres. In the upper left hand corner of each image is the total ion TOF-SIMS image and below that is the fluorescence microscopy image of the same area. The total ion image for all the samples we analyzed was dominated by topographic effects which resulted in a bright region on the left side of the spheres and an ion shadow on the right edge of the spheres. There is some distortion in the images which results from the incidence angle of the primary ion beam.

MAF analysis of the two images shown in Figs. 1 and 2 revealed three significant factors both when the full peak set was used and when only the amino acid fragments listed in Table I were used. For both images and both data sets the first factor described differences between the spheres and the silicon substrate, the second factor showed variations in total ion yield resulting from the topography of the samples and the third factor (Figs. 1 and 2 right) revealed contrast between two different types of spheres. The spheres which appear “green” and “red” in the MAF images correspond to the green and red spheres in the fluorescence image, which

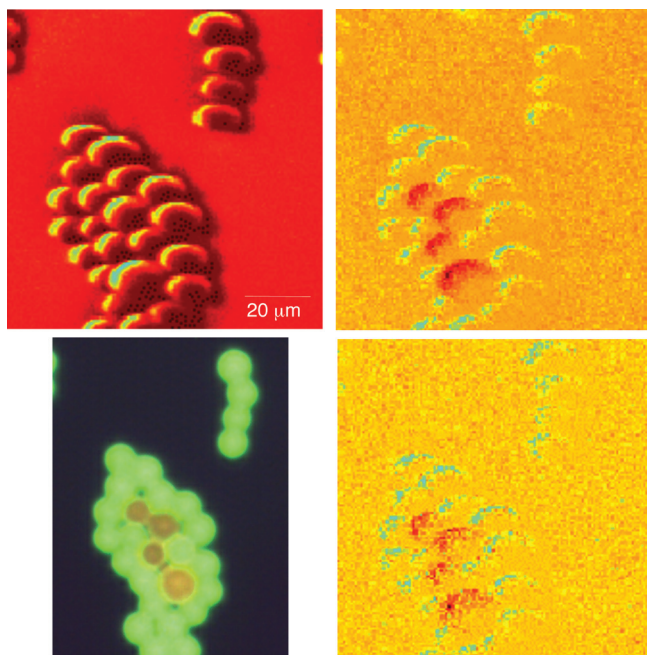


FIG. 1. (Color) Images of sample 1 which consists of BSA adsorbed onto green fluorescent microspheres and hemoglobin adsorbed onto red fluorescent microspheres. The total ion TOF-SIMS image (upper left) reveals topography. MAF images calculated using 321 peaks (upper right) and 34 amino acid peaks (lower right) mirror the contrast observed in the fluorescence image (lower left).

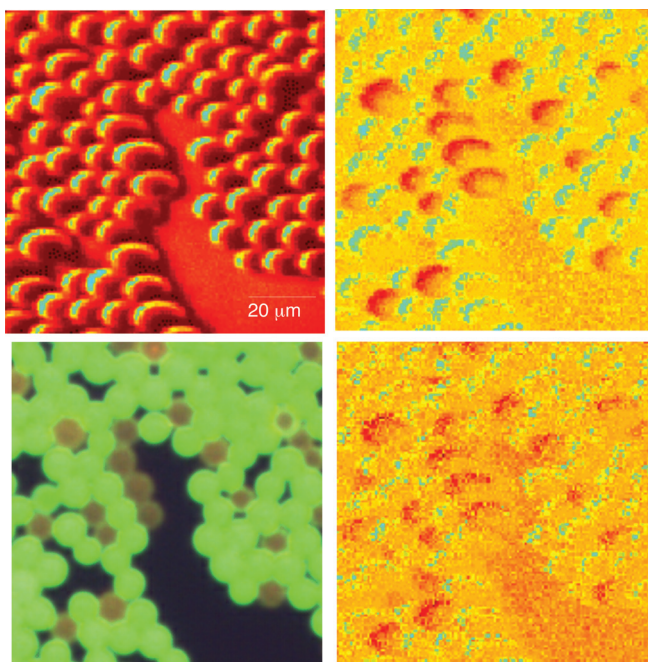


FIG. 2. (Color) Images of sample 2 which consists of BSA adsorbed onto green fluorescent microspheres and hemoglobin adsorbed onto red fluorescent microspheres. The total ion TOF-SIMS image (upper left) reveals topography. MAF images calculated using 321 peaks (upper right) and 34 amino acid peaks (lower right) mirror the contrast observed in the fluorescence image (lower left).

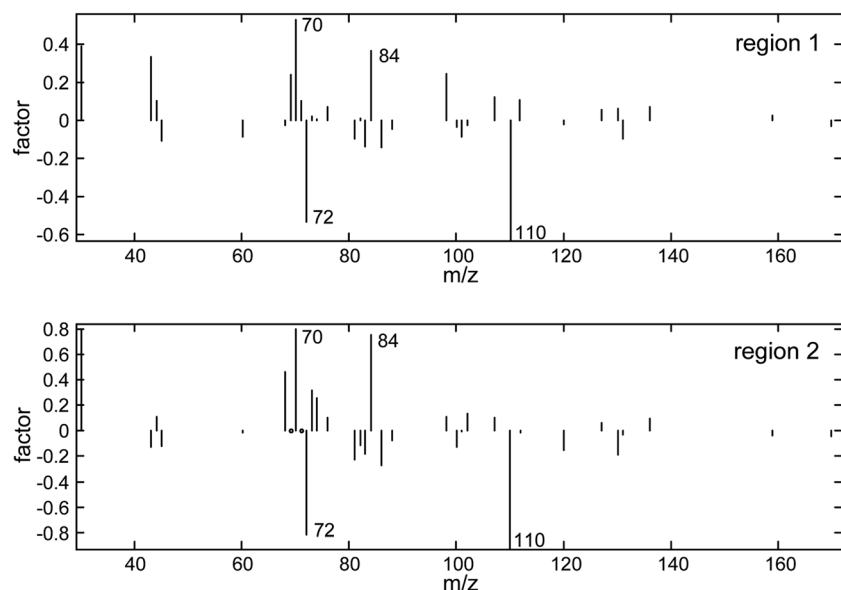


FIG. 3. Pseudospectra calculated by MAF using the 34 amino acid peaks for two samples consisting of BSA and hemoglobin coated microspheres. The top graph corresponds to the image in Fig. 1 and the lower graph corresponds to the image in Fig. 2.

supports the conclusion that this factor describes differences between the hemoglobin coated red fluorescent spheres and BSA coated green fluorescent spheres. MAF factor 3 for the full data (Figs. 1 and 2, top right) shows better contrast between the spheres than when only the amino acid fragments are included in the analysis (Figs. 1 and 2, bottom right); however, the contrast in the amino acid only image is adequate to correctly classify each of the spheres.

Figure 3 shows the MAF pseudospectra associated with the factor 3 images calculated using only the amino acid peaks. The pseudospectra associated with Fig. 1 is shown at the top while the “spectra” for Fig. 2 is shown below. Positive intensity peaks in the pseudospectra correspond to the green (BSA) areas in the images while negative intensity peaks are predominant in the red (hemoglobin) areas of the images. The spectra have a high degree of similarity and the most intense positive peaks ( $m/z$  70 and  $m/z$  84) and negative peaks ( $m/z$  72 and 110) in the two spectra are identical. Minor differences between these pseudospectra arise from the differences in the fraction of the silicon substrate that is covered by the spheres. The key negative intensity peaks,  $m/z = 72$  and  $m/z = 110$ , correspond to the amino acid residues valine and histidine. The key positive intensity peak at  $m/z = 70$  can arise from either asparagine or proline, and the positive peak at  $m/z = 84$  can arise from glutamine, glutamic acid, or lysine. Table II shows the amino acid composition of the three proteins considered in this study. As can be seen in this table, hemoglobin has a significantly higher level of valine and histidine, while BSA is higher in glutamine, glutamic acid, lysine and proline. This pattern in the study spectra further supports the hypothesis that the factor 3 MAF images are revealing differences in the adsorbed proteins on the spheres.

To further verify this relationship, a third region from the same sample was analyzed. Rather than process this image

directly with MAF, the MAF factor 3 loadings, which were calculated from the region shown in Fig. 2, were applied directly to this image. The results are shown in Fig. 4. In the upper left is the image calculated using the full peak set and the image calculated using only the amino acid peaks is shown in the upper right. As a final test, MAF analysis was performed on this image using only the four key peaks ( $m/z = 70, 72, 84,$  and  $110$ ) identified in the analysis of the first two regions. The resulting MAF factor 2 image is shown in

TABLE II. Amino acid composition of studied proteins.

Amino acid	Bovine serum albumin (BSA)	Human serum albumin (HSA)	Hemoglobin (Hg)
Ala (A)	7.9%	10.3%	12.6%
Arg (R)	4.3%	4.1%	2.4%
Asn (N)	2.3%	2.8%	3.5%
Asp (D)	6.6%	5.9%	5.9%
Cys (C)	5.8%	5.9%	0.3%
Gln (Q)	3.3%	3.3%	0.2%
Glu (E)	9.7%	10.0%	4.5%
Gly (G)	2.8%	2.6%	7.0%
His (H)	2.8%	2.6%	5.6%
Ile (I)	2.5%	1.5%	0.0%
Leu (L)	10.7%	10.5%	12.9%
Lys (K)	9.9%	9.9%	8.4%
Met (M)	0.8%	1.1%	1.4%
Phe (F)	4.9%	5.9%	5.9%
Pro (P)	4.6%	3.9%	3.5%
Ser (S)	5.3%	4.6%	6.3%
Thr (T)	5.6%	4.8%	4.9%
Trp (W)	0.5%	0.3%	1.0%
Tyr (Y)	3.5%	3.0%	1.7%
Val (V)	6.3%	6.9%	10.5%

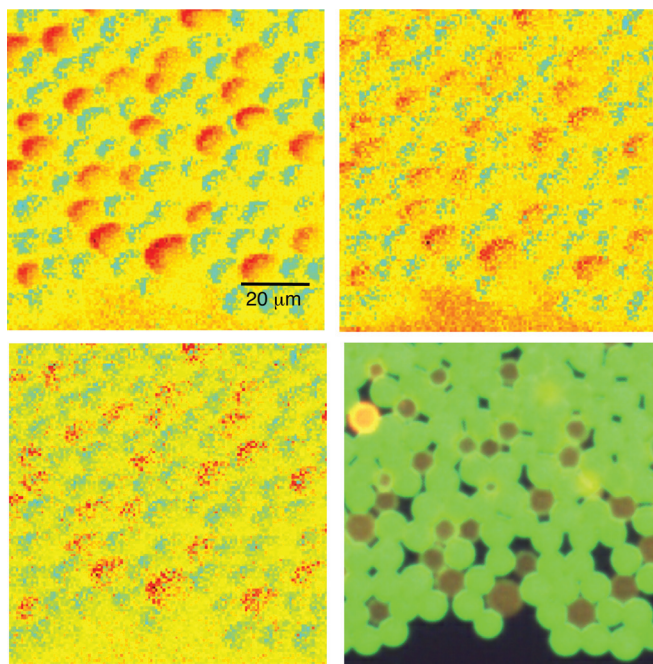


FIG. 4. (Color) Images for sample 3 obtained using the MAF loadings calculated for sample 2. On the upper left, results for the full peak set are shown. The MAF images calculated using 321 peaks (upper left), 34 amino acid peaks (upper right), and only the 4 key amino acid peaks (lower left) mirror the contrast observed in the fluorescence image (lower right).

the bottom left in Fig. 4. A comparison of these three images to the fluorescence image shown in the bottom right in Fig. 4 verifies that the same relationships hold for this region as for the previously analyzed images providing further evidence that TOF-SIMS is revealing differences between the two proteins adsorbed to the spheres.

Figure 5 shows images obtained from a sample of BSA and HSA coated spheres. As can be seen in Table II, BSA and HSA have a greater similarity than BSA and hemoglobin. Although the proteins have much greater similarity, clear contrast between the BSA coated green fluorescent spheres and the HSA coated red fluorescent spheres is still evident in the MAF factor 3 images calculated using both the full peak set and the amino acid peak set. Figure 6 shows the MAF factor 3 pseudospectra calculated using the amino acid peak set. Positive intensity peaks in the pseudospectra correspond to the green (BSA) areas in the images while negative intensity peaks are predominant in the red (HSA) areas of the images. The key negative intensity peaks can be attributed to the amino acids alanine ( $m/z=44$ ), arginine ( $m/z=43$ ,  $m/z=73$ , and  $m/z=127$ ), and valine ( $m/z=72$ ). These amino acids all have a higher concentration in HSA than in BSA. The key positive peaks in the pseudospectra can be assigned to proline ( $m/z=68$ ), threonine ( $m/z=74$ ), and histidine ( $m/z=110$ ) which are all elevated in BSA. The pseudospectra associated with the MAF factor 3 image calculated from the full data set shows significant contribution from peaks other than the key amino acid peaks. These features of the pseudospectra are consistent with the image contrast between BSA and HSA coated spheres.

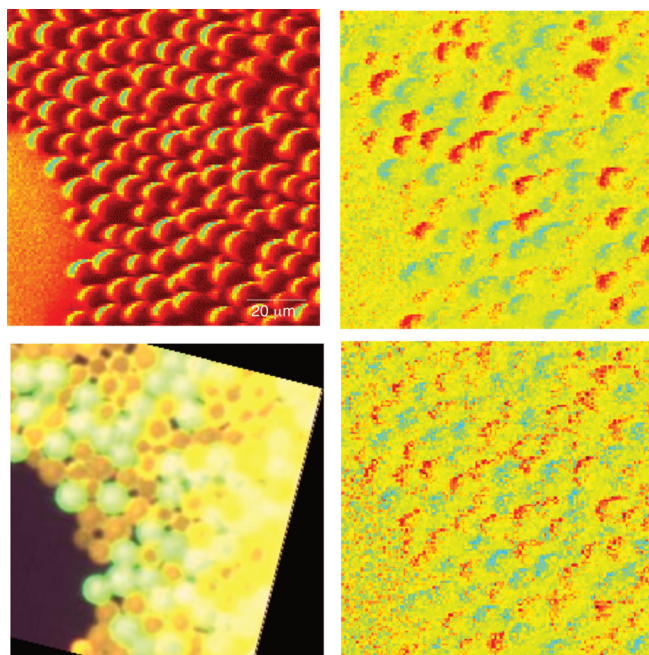


FIG. 5. (Color) Images of sample 4 which consists of BSA adsorbed onto green fluorescent microspheres and HSA adsorbed onto red fluorescent microspheres. The total ion TOF-SIMS image (upper left) reveals topography. The MAF images calculated using 321 peaks (upper right) and 34 amino acid peaks (lower right) mirror the contrast observed in the fluorescence image (lower left).

Although the analysis of the amino acid only peak set, indicates that TOF-SIMS is sensitive to the small differences between these two proteins, it is not possible to rule out enhanced contrast due to either differences in the total amounts of adsorbed protein or differences in the fluorescent labeled microspheres. When the full data set is analyzed, the highest intensity peak in this pseudospectra is at  $m/z=91$ , which most likely arises from the polystyrene microsphere rather than the adsorbed protein layer. This suggests that at least part of the contrast observed in this image may result from differences in chemistry between the red and green fluorescently labeled microspheres rather than the chemical differences in the proteins themselves.

In previous studies, Wagner *et al.* compared  $\text{Cs}^+$  TOF-SIMS spectra of BSA, HSA, hemoglobin and ten other proteins using PCA<sup>24</sup> and LDA<sup>18</sup> adsorbed to mica and Teflon. They found that with the aid of PCA all of the proteins could be accurately identified based on the amino acid fragments observed in the TOF-SIMS spectra. In that study, however, only spectra from large, presumably uniform areas were used. It is unclear from their results whether the differences between the proteins were large enough to provide adequate contrast in low signal to noise ratio images particularly if confounding topography was present. They found that TOF-SIMS spectra of hemoglobin could be easily separated from TOF-SIMS spectra of BSA and the peaks responsible for this separation could be easily related to known differences in the amino acid composition of the two proteins. In their work, the key peaks identified for separating BSA and hemoglobin were  $m/z=72$  (valine) and  $m/z=110$  (histidine)

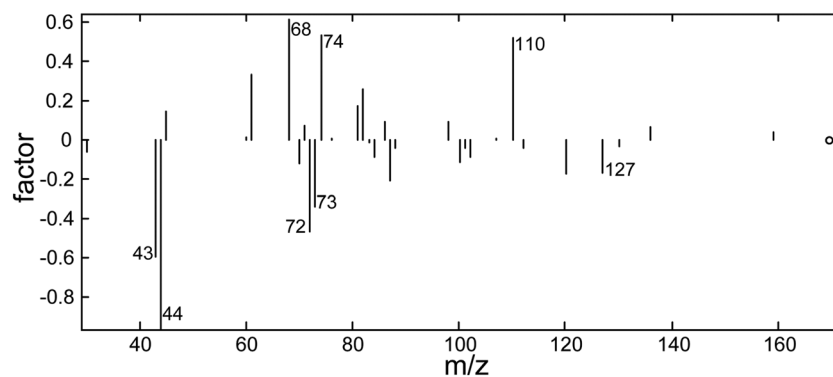


FIG. 6. Pseudospectrum calculated by MAF using the 34 amino acid peaks for samples 4 (Fig. 5) which consists of BSA and HSA coated microspheres.

which were more intense in the hemoglobin spectra as well as  $m/z = 70$  (proline) and  $m/z = 84$  (lysine) which were more intense in the BSA spectra. Although our study has been done at lower mass resolution, our results for the images are consistent with Wagner's results for spectra from large uniform areas. This result is particularly significant considering the differences in the primary ion source used and the different substrate beneath the proteins.

Wagner *et al.* also found some statistically significant separation between spectra of HSA and BSA, however, this separation was not clean with significant overlap between the two groups and no clear relationship between the PCA loadings and the known differences in the amino acid composition. Given Wagner's limited success in separating HSA and BSA, it is of particular note that we have been able to obtain clear contrast between these two proteins in this study. The enhanced ability to distinguish these very similar proteins is likely due to the  $\text{Bi}_3^+$  primary ion.

To address the concern that image contrast was the result of the different fluorescent labels rather than the differences between the adsorbed proteins, two further images have been analyzed. For these samples, HSA and hemoglobin were both adsorbed onto the green fluorescent microspheres, mixed together, and then deposited onto silicon substrates for TOF-SIMS analysis. The raw data files were processed as described above and then the image stacks were analyzed using MAF. For these two samples, only 2 MAF factors were found to be significant because none of the silicon substrate is visible in the images. Results for MAF factor 2 for the full peak set and amino acids are shown in Fig. 7. At the top are the images calculated using the full peak sets and the images calculated using only the amino acid peaks. Two classes of spheres can be clearly identified in both samples. Contrast between these spheres is evident using either the full data set or only the characteristic amino acid fragments. For both of these images, the most intense positive peaks in the pseudospectra, which correspond to the green spheres in the MAF images, arise from alanine ( $m/z = 44$ ) and valine ( $m/z = 72$ ) suggesting that these are the hemoglobin coated spheres; however, differences in other regions of the pseudospectra make a definitive identification difficult without the fluorescent labels.

To better identify the proteins on the unlabeled spheres in Fig. 7, spectra were constructed from 321 spheres from Figs.

1 and 2, 4 and 5 whose protein coat could be identified by the fluorescent labels. A linear discriminant analysis of this data set was performed using the 34 amino acid peaks to identify combinations of the peaks that best separated the three proteins.<sup>18</sup> Spectra from the spheres seen in the two images in Fig. 7, where the protein could not be identified using the fluorescence image, were then projected on to the same linear discriminant axis. The results are shown in Fig. 8. Discriminant scores for the spheres which appear green in the MAF analysis (Fig. 7) are plotted as circles and those which appear red in the MAF analysis are plotted as squares. As can be seen in Fig. 8, comparison with the known samples allows clear identification of both the hemoglobin and HSA coated spheres. It is notable that the HSA coated on green fluorescent spheres cluster with the HSA coated red fluorescent spheres and can be clearly distinguished from BSA coated green fluorescent spheres demonstrating that the key

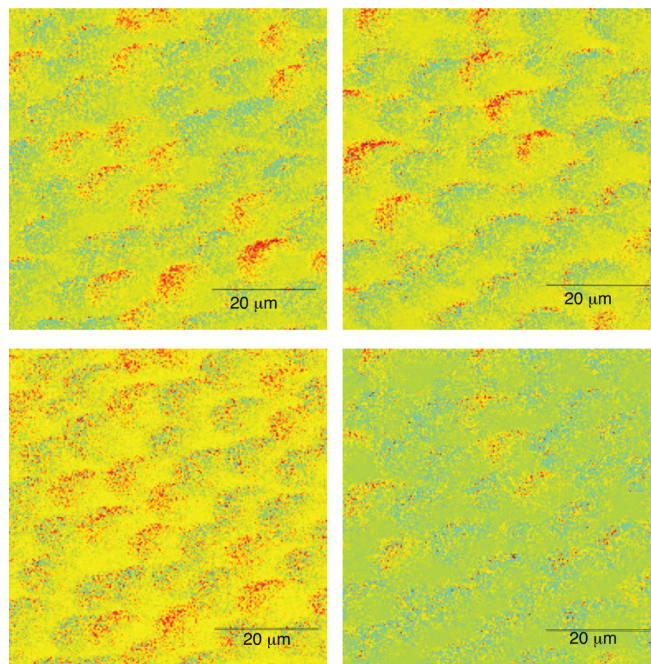


FIG. 7. (Color) MAF images of samples 5 (left) and 6 (right) which consist of BSA and HSA adsorbed onto green fluorescent microspheres. Images on the top row were calculated using the 321 peak data set. Those on the bottom row were calculated using only the 34 amino acid peaks.

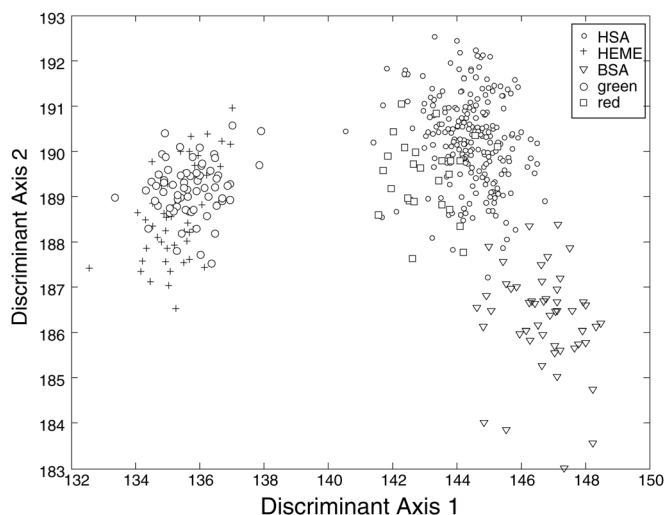


FIG. 8. Results from linear discriminant analysis of the protein coated spheres. The discriminant model was built using spectra from hemoglobin (+), HSA (●), and BSA (▽) coated spheres that could be identified based on the fluorescent images. Points marked with  $\nu$  and  $\lambda$  are for spheres that could not be identified from the fluorescent images.

differences observed are in fact the results of differences between the proteins and not the underlying substrate.

#### IV. CONCLUSIONS

By using the  $\text{Bi}_3^+$  primary ion source, we have successfully imaged  $10\ \mu\text{m}$  protein features in the presence of complex topographic effects. With MAF processing, images showed clear contrast between both the very different proteins (HSA and hemoglobin) and the very similar proteins (HSA and BSA). Similar results were obtained with and without the fluorescent labels. MAF images were calculated using both the full spectrum and previously identified amino acid peaks. Although better image contrast was obtained using the full spectrum, differences between the spheres were still evident when only the amino acid fragments were included in the analysis, indicating that we are truly observing differences between the proteins themselves. Key peaks in the pseudospectra associated with the MAF images can be easily related to differences in the amino acid composition of the proteins and are consistent with previously published TOF-SIMS analysis of proteins. The  $\text{Bi}_3^+$  source showed clear advantages when compared to our previous work using  $\text{Ga}^+$ . The HSA/BSA results showed improvements over previous protein TOF-SIMS analyses using  $\text{Cs}^+$ . These results demonstrate that TOF-SIMS, with a  $\text{Bi}_3^+$  primary ion, is a powerful technique for characterizing interfacial proteins not only on large uniform surfaces, but also with high spatial resolution on the topographically complex samples typical in biological analysis.

#### ACKNOWLEDGMENTS

This work was generously funded by NIH Grant No. EB-002027 and the European Commission under Contract No. 005045 (FP6).

- <sup>1</sup>T. A. Horbett, *Colloids Surf.*, **B 2**, 225 (1994).
- <sup>2</sup>T. O. Collier, C. H. Thomas, J. M. Anderson, and K. E. Healy, *J. Biomed. Mater. Res.* **49**, 141 (2000).
- <sup>3</sup>J. A. Hubbell, *Curr. Opin. Biotechnol.* **14**, 551 (2003).
- <sup>4</sup>D. Lindsay and A. von Holy, *J. Hosp. Infect.* **64**, 313 (2006).
- <sup>5</sup>M. A. Daeschel and J. McGuire, *Biotechnol. Genet. Eng. Rev.* **15**, 413 (1998).
- <sup>6</sup>J. D. Bryers, *Biotechnol. Bioeng.* **100**, 1 (2008).
- <sup>7</sup>Y. F. Dufrene, C. J. Boonaert, and P. G. Rouxhet, *Methods Enzymol.* **310**, 375 (1999).
- <sup>8</sup>M. D. McKee and A. Nanci, *Connect. Tissue Res.* **35**, 197 (1996).
- <sup>9</sup>C. J. Wilson, R. E. Clegg, D. I. Leavesley, and M. J. Percy, *Tissue Eng.* **11**, 1 (2005).
- <sup>10</sup>S. Aoyagi and M. Kudo, *Biosens. Bioelectron.* **20**, 1626 (2005).
- <sup>11</sup>O. Iguer, C. Poleunis, F. Mazeas, C. Compere, and P. Bertrand, *Langmuir* **24**, 12272 (2008).
- <sup>12</sup>A. Tang, C. Wang, R. Stewart, and J. Kopecek, *Bioconjug. Chem.* **11**, 363 (2000).
- <sup>13</sup>D. Belazi, S. Sole-Domenech, B. Johansson, M. Schalling, and P. Sjoval, *Histochem. Cell. Biol.* **132**, 105 (2009).
- <sup>14</sup>Y. K. Magnusson, P. Friberg, P. Sjoval, J. Malm, and Y. Chen, *Obes. (Silver Spring)* **16**, 2745 (2008).
- <sup>15</sup>M. J. Baker, L. Zheng, N. Winograd, N. P. Lockyer, and J. C. Vickerman, *Langmuir* **24**, 11803 (2008).
- <sup>16</sup>Y. Wu, F. I. Simonovsky, B. D. Ratner, and T. A. Horbett, *J. Biomed. Mater. Res. A* **74**, 722 (2005).
- <sup>17</sup>P. Tengvall, I. Lundstrom, and B. Liedberg, *Biomaterials* **19**, 407 (1998).
- <sup>18</sup>M. S. Wagner, B. J. Tyler, and D. G. Castner, *Anal. Chem.* **74**, 1824 (2002).
- <sup>19</sup>R. A. Caldwell, J. E. Woodell, S. P. Ho, S. W. Shalaby, T. Boland, E. M. Langan, and M. LaBerge, *J. Biomed. Mater. Res.* **62**, 514 (2002).
- <sup>20</sup>J. R. Smith, M. T. Cicerone, and C. W. Meuse, *Langmuir* **25**, 4571 (2009).
- <sup>21</sup>F. Cheng, L. J. Gamble, and D. G. Castner, *Anal. Chem.* **80**, 2564 (2008).
- <sup>22</sup>C. Brüning, S. Hellweg, S. Dambach, D. Lipinsky, and H. F. Arlinghaus, *Surf. Interface Anal.* **38**, 191 (2006).
- <sup>23</sup>B. A. Gotliv and A. Veis, *Cells Tissues Organs* **189**, 12 (2009).
- <sup>24</sup>J. B. Lhoest, M. S. Wagner, C. D. Tidwell, and D. G. Castner, *J. Biomed. Mater. Res.* **57**, 432 (2001).
- <sup>25</sup>M. S. Wagner, T. A. Horbett, and D. G. Castner, *Biomaterials* **24**, 1897 (2003).
- <sup>26</sup>M. S. Wagner, S. L. McArthur, M. Shen, T. A. Horbett, and D. G. Castner, *J. Biomater. Sci. Polym. Ed.* **13**, 407 (2002).
- <sup>27</sup>M. S. Wagner, M. Shen, T. A. Horbett, and D. G. Castner, *J. Biomed. Mater. Res. A* **64**, 1 (2003).
- <sup>28</sup>Y. P. Kim, M. Y. Hong, J. Kim, E. Oh, H. K. Shon, D. W. Moon, H. S. Kim, and T. G. Lee, *Anal. Chem.* **79**, 1377 (2007).
- <sup>29</sup>K. Leufgen, M. Mutter, H. Vogel, and W. Szymczak, *J. Am. Chem. Soc.* **125**, 8911 (2003).
- <sup>30</sup>A. M. Belu, D. J. Graham, and D. G. Castner, *Biomaterials* **24**, 3635 (2003).
- <sup>31</sup>H. E. Canavan, X. Cheng, D. J. Graham, B. D. Ratner, and D. G. Castner, *J. Biomed. Mater. Res. A* **75**, 1 (2005).
- <sup>32</sup>C. Y. Lee, G. M. Harbers, D. W. Grainger, L. J. Gamble, and D. G. Castner, *J. Am. Chem. Soc.* **129**, 9429 (2007).
- <sup>33</sup>S. Rangarajan and B. J. Tyler, *Appl. Surf. Sci.* **231**, 406 (2004).
- <sup>34</sup>R. De Mondt, L. Van Vaecck, A. Heile, H. F. Arlinghaus, N. Nieuwjaer, A. Delcorte, P. Bertrand, J. Lenaerts, and F. Vangaever, *Rapid Commun. Mass Spectrom.* **22**, 1481 (2008).
- <sup>35</sup>D. Touboul, F. Kollmer, E. Niehuis, A. Brunelle, and O. Laprevote, *J. Am. Soc. Mass Spectrom.* **16**, 1608 (2005).
- <sup>36</sup>M. Wagner, A. Loy, R. Nogueira, U. Purkhold, N. Lee, and H. Daims, *Antonie van Leeuwenhoek* **81**, 665 (2002).
- <sup>37</sup>B. J. Tyler, *Appl. Surf. Sci.* **252**, 6875 (2006).
- <sup>38</sup>B. J. Tyler, G. Rayal, and D. G. Castner, *Biomaterials* **28**, 2412 (2007).